Bachelor's project

Kjetil Langelid
Ole Martin Sørensen

Effect of Wind Shear and Turbulence on Wind Turbine Power Production, Based on LIDAR Measurements

NTNU
Norwegian University of Science and Technology
Faculty of Engineering
Department of Energy and Process Engineering

NTNU
Kunnskap for en bedre verden

Kjetil Langelid
Ole Martin Sørensen

Effect of Wind Shear and Turbulence on Wind Turbine Power Production, Based on LIDAR Measurements

NTNU

Kunnskap for en bedre verden

Bachelor Thesis

Thesis Title:	Date:
Effect of Wind Shear and Turbulence on Wind Turbine Power Production, Based on LIDAR Measurements	22.05.20
Authors:	Supervisor:
Kjetil Langelid and Ole Martin Sørensen	Tania Bracchi
Field of Study:	Thesis Number:
Renewable Energy, Engineering	FEN 3001-2011
Employer:	Contact Person:
TrønderEnergi	Lina Nordaune

Preface

This bachelor's thesis was written at the Department of Energy and Process Engineering at the Norwegian University of Science and Technology (NTNU), completing a three-year bachelor's degree in Renewable Energy.

We want to thank our supervisor Tania Bracchi for support and guidance throughout the semester. She has helped us approach this thesis with her broad understanding of wind engineering.

We also want to thank TrønderEnergi and, in particular, Lina Nordaune for giving access to data, sharing her experiences and the chance to write this thesis.

Additionally, we want to thank the team at Simis for quick and helpful support during the simulation process.

And lastly, we want to thank John Kåre Langelid and Elias Syslak for perusal and constructive feedback.

Trondheim, 22.05.20

Ole Martin Sørensen	Kjetil Langelid
Student ID: 476019	Student ID: 493031

Abstract

During the work of this bachelor's thesis, the power performance of a multi-megawatt wind turbine equipped with a continuous wave LIDAR was analyzed. LIDAR measurements were used to calculate wind shear and turbulence intensity to complement the turbine data. Numerous conditions filtered the entire data set to increase the reliability of results. Large intervals of data were dropped due to unreliable LIDAR measurements.

Simulations were run for various shear exponents and turbulence intensities. Wind shear simulations yielded minor changes in power output for increasing wind velocities. Power curves created for high wind shears dropped below the ones estimated for lower wind shears, reducing AEP. Turbulence simulations resulted in power curves with significant deviations. High turbulence intensities over-performed for low wind velocities but dropped substantially with increasing wind velocity. Power curves calculated for high turbulence intensities lead to a reduction in AEP.

Turbine data were binned into four ranges of shear exponents: $\alpha < 0$, $0 \leq \alpha < 0.1$, $0.1 \leq \alpha < 0.25$, and $\alpha \geq 0.25$. This resulted in power curves that corresponded well with simulations. Low and positive wind shear yielded highest AEP, with $\alpha < 0$, $0.1 \leq \alpha < 0.25$, and $\alpha \geq 0.25$ being reduced with 0.8%, 0.5%, and 0.8%, respectively. Data binned by turbulence intensity deviated significantly. Power curves for four turbulence intensities were calculated: $0 \leq TI < 0.06$, $0.06 \leq TI < 0.12$, $0.12 \leq TI < 0.18$, and $TI \geq 0.18$. These power curves corresponded relatively well with simulations, following the same trend. Power curves for higher turbulence intensities lead the ones for lower turbulence intensities at low wind velocities. Power output for velocities above 9 m/s were significantly better for lower turbulence intensities. Compared to the reference range $0 \leq TI < 0.06$, AEP was reduced with 0.6%, 1.1%, and 1.4% for $0.06 \leq TI < 0.12$, $0.12 \leq TI < 0.18$, and $TI \geq 0.18$, respectively.

Contents

List of Figures

List of Tables

Abbreviations

AEP	Annual Energy Production
BEM	Blade Element Momentum theory
DSM	Direction Section Management
FFT	Fast Fourier Transform
IEC	International Electrotechnical Commission
LIDAR	Light Detection And Ranging
LOS	Line of Sight
NREL	National Renewable Energy Laboratory
PDF	Probability Density Function
PI	Proportional-Integral
PID	Proportional–Integral–Derivative
RMSE	Root Mean Square Error
RPM	Rounds per Minute
SCADA	Supervisory Control And Data Acquisition
STD	Standard Deviation
TI	Turbulence intensity
TSR	Tip Speed Ratio

1 Introduction

According to NVE, the influence of wind turbines in Norway are ever-increasing. In 2016 wind energy accounted for 1,4 % of the total electricity production in Norway. At the end of 2019, this was increased to 4%, producing 5.5 TWh. This increase is a result of growing demand for green energy. It is crucial to push for a sustainable future by favoring renewable energy sources when meeting demand. Increasing efficiency and reducing costs are two important factors when chasing the green shift. [1]

Studying wind turbine characteristics is, therefore, essential to optimize efficiency and reduce operating costs. Turbulence and wind shear are two factors influencing wind turbine power performance and structural load. This thesis analyses how turbulence and wind shear affect wind turbine power production.

LIDAR measurements were averaged over ten-minute periods and collated with turbine data. Turbulence intensities and wind shears for each period were calculated. Data was eventually binned by their respective turbulence intensity or wind shear values and analyzed. The theory and concepts used throughout the thesis are explained in section 2. Section 3 describes how data was handled, filtered, and then analyzed. The results from this section can be found in section 4, before these results are discussed in section 5. Conclusions are presented in the final section, 6.

2 Theory

For the ever-growing energy market, efficiency is crucial from an economic point of view, but also to ensure sustainable development of power production when meeting increasing market demand. Knowledge about characteristics that might affect the efficiency of power production from wind turbines, like wind shear and turbulence, is therefore of greater significance. This section gives a brief introduction to some of the concepts and techniques applied in this thesis. Highlighting these few subsections of theories is done to substantiate the decisions and reasoning behind methods used to process data and conclusions drawn from measurements, and also to give a brief introduction to wind power production.

2.1 Power Production from Wind Turbines

The law of conservation of energy states that the total energy of an isolated system is constant. Energy can neither be created nor destroyed, only transform from one form to another. When harvesting energy from the wind, this law of conservation applies. Wind flowing through a turbine will generate mechanical energy by transferring some of its kinetic energy to the the turbine. The rotation of the blades will drive a generator, converting the mechanical energy into electricity. [2, 3]

By analyzing a turbine following several assumptions, such as no frictional drag, a non-rotating wake, and homogeneous, incompressible, steady-state flow, air flowing through a turbine can be examined in a control volume, created by fictive stream tube boundaries. Air flowing towards a turbine with a given velocity will lose some of its velocity or kinetic energy due to work done on the turbine. The stream tube boundaries behind the turbine will increase as a result of decreased velocity. By extracting more energy, the velocity behind the turbine will eventually become so small compared to the initial velocity, that it will prevent the incoming flow to reach the turbine. The optimal velocity ratio between incoming flow and downstream flow is found to be $1/3$. This results in the theoretical limit of a turbine's power coefficient, or Betz limit, equal to 0.593. [2, 4]

The power coefficient C_P of a wind turbine is described as the ratio between power extracted at the rotor plane and available wind power through the turbine's sweeping area, as shown in equation 2.1. Here P_{rotor} is rotor power, ρ is the density of air, U is wind velocity, and A is the sweeping area. [2]

$$C_P = \frac{P_{rotor}}{\frac{1}{2}\rho U^3 A} \tag{2.1}$$

Even though the theoretical maximum value for the power coefficient is relatively high, three main factors lead to a decrease in the maximum achievable power coefficient:

- wake rotation behind the rotor

- finite number of blades with corresponding tip losses

- aerodynamic drag

Smaller factors like turbulence and wind shear also contribute to lower power output for wind turbines. These factors can, over time, lead to considerable reductions in AEP. The overall efficiency of a wind turbine is the product of the

1

associated power coefficient and mechanical efficiency, which includes mechanical and electrical losses in gearbox and generator. Today, a modern wind turbine extract between 30-40% of the wind energy passing through the sweeping area. [2, 3]

2.2 Turbulence

2.2.1 Turbulence Intensity

Turbulence in the wind is a phenomenon caused by the conversion of kinetic energy to thermal energy through the creation and destruction of smaller gusts or eddies. A turbulent wind profile may have a reasonably constant mean velocity over more extended periods but is subject to frequent variations over shorter periods, like minutes or seconds. Changes in a wind profile caused by turbulence are seemingly random. However, some features of turbulence can be characterized using statistical properties like turbulence intensity. [2]

Turbulent wind can be described as a three dimensional vector consisting of longitudinal, lateral, and vertical wind components, designated $u(z,t)$, $v(z,t)$ and $w(z,t)$ respectively. Each of these components is thought of as short-term mean wind with a turbulent component added to them, as shown in equation 2.2, z is the height above ground, t is time and lower case u, v or w is instantaneous wind velocity. [2]

$$u(z,t) = U + \widetilde{u}(z,t), \qquad v(z,t) = V + \widetilde{v}(z,t), \qquad w(z,t) = W + \widetilde{w}(z,t) \tag{2.2}$$

The short-time average U, V, or W are usually calculated over ten minutes. Equation 2.3 shows how the longitudinal wind component U is averaged with N number of samples. [2]

$$U = \frac{1}{N} \sum_{i=1}^{N} u_i \tag{2.3}$$

Turbulence intensity is defined as the ratio between the standard deviation of the wind velocity and the mean wind velocity given in equation 2.3. The standard deviation of wind component u is given in equation 2.4. [2]

$$\sigma_u = \sqrt{\frac{1}{N-1} \sum_{i=1}^{N} (u_i - U)^2} \tag{2.4}$$

These calculations are done over a time interval of ten minutes by convention in wind energy engineering, with a sampling rate of 1 Hz or more. Turbulence intensity or TI is defined in equation 2.5. Turbulence intensity is often found in the 0.1 to 0.4 range, with higher turbulence intensity typically occurring at lower wind velocities. High, medium, and low turbulence intensities are commonly referred to as A, B, and C with corresponding values of 0.16, 0.14, 0.12. [2]

$$TI = \frac{\sigma_u}{U} \tag{2.5}$$

2.2.2   The Kaimal Model

Turbulence can also, to some extent, be characterized in the frequency domain. Low-frequency components dominate turbulent fluctuations, with high-frequency components having less influence. It is developed several spectral models to represent turbulence in the frequency domain, one of them beeing the IEC Kaimal model. According to NREL, this model is defined in IEC 61400-1, and the velocity spectra for all three wind components, k = u, v, w, are given in equation 2.6. [8]

$$S_k(f) = 4\sigma_k^2 \frac{L_k/\bar{u}_{hub}}{(1 + 6fL_k/\bar{u}_{hub})^{5/3}} \tag{2.6}$$

Here f is cyclic frequency, L_k is the integral scale parameter given in equation 2.9, and $\bar{u}_{hub}$ is longitudinal mean wind velocity at hub height. [8, 9]

$$L_k = \begin{cases} 8.10\Lambda_U, & k = u \\ 2.70\Lambda_U, & k = v \\ 0.66\Lambda_U, & k = w \end{cases} \tag{2.9}$$

The turbulence parameter Λ_U is defined in equation 2.10. Note that $min(60m, z_{hub})$ indicates the minimum value of 60m and hub height. [8, 9]

$$\Lambda_U = 0.7 \cdot min(60m, z_{hub}) \tag{2.10}$$

The relationship between standard deviations are finally given in equation 2.11. [8, 9]

$$\sigma_v = 0.8\sigma_u, \qquad \sigma_w = 0.5\sigma_u \tag{2.11}$$

This method is later used in this thesis to run turbulence simulations, which is described in section 3.3.4. [8, 9]

2.3   Wind Shear

2.3.1   Atmospheric Boundary Layer and Wind Shear

The atmospheric boundary layer is the lowest part of the earth's atmosphere. The characteristics of this part of the atmosphere are heavily influenced by contact with the earth's surface. Variables such as wind velocity, direction, temperature, and humidity can have large variations within relatively small changes in time and space. A critical characterization of the wind resource is the change in wind velocity with height. Wind at level with earth's surface is expected to have zero velocity as a consequence of friction. As one moves away from the surface, the wind velocity increases, creating a vertical wind profile. This vertical profile is called wind shear and is essential in wind engineering for two main reasons. Firstly, it directly affects power production from a wind turbine. And secondly, it causes stress on the wind turbine's blades as the rotor is rotating in a varying wind field, creating cyclic loads. [2, 3]

An important property of the atmosphere is its tendency to suppress vertical motion or turbulence, stabilizing itself. The atmosphere's stability is mainly governed by the varying temperature at different heights and is a decisive factor for the wind shear created in the atmospheric boundary layer. A stable atmosphere less affected by turbulence will have a smoother vertical wind profile. Still, the actual wind profile will always be affected by local variations in wind velocity and direction, as shown in figure 2.1. [2]
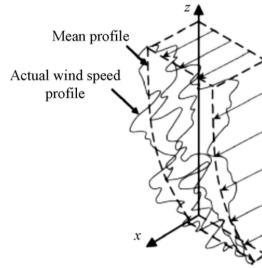
Figure 2.1: *Illustration of mean and actual wind profiles [2]*

The distribution of varying temperatures in the boundary layer is referred to as thermal stratification. Heated air is more buoyant than cooled air. The temperature distribution in the boundary layer will, therefore, be the leading cause of turbulence. The more significant the difference in temperature, the more turbulence is formed. As warm air rises, the difference in wind velocity at different heights will equalize, creating a more uniform wind profile. How heavily thermal stratification influence the vertical wind profile depends on time and space. As the ground has a low heat capacity compared to the sea, the impact of thermal stratification is expected to be larger onshore than offshore. The same applies for night and day, as the sun heats the surface during the day, reducing wind shear. [5]

2.3.2   Wind Shear Profiles Using the Power Law

The power law is a simple model widely used by energy researchers to estimate a vertical wind velocity profile between two heights. When exploring a wind profile in the atmospheric boundary layer, it is important to acknowledge that this law has, in general, been used to model wind profiles over regions with uniform, flat terrain. Wind profiles over more complex terrain will be exposed to uncertainty caused by turbulent flows. The power law is given in equation 2.7. Here $U(z)$ and $U(z_r)$ are wind velocity at the desired height and reference height, z and z_r are height and reference height, and α is the power law exponent. [2, 6]

$$\frac{U(z)}{U(z_r)} = \left(\frac{z}{z_r}\right)^{\alpha} \tag{2.7}$$

The power law exponent α or shear exponent relates wind velocities at two different heights. The shear exponent has been found to vary with different parameters like elevation, atmospheric stability, temperature, and time of day. A large shear exponent corresponds to a large vertical gradient in the vertical velocity profile. [2, 6]

Figure 2.2 illustrates how the power law predicts the per unit wind velocity to develop with height. Higher shear exponents yield a larger change in wind velocity at a given height compared to the reference height at 10 m. [7]
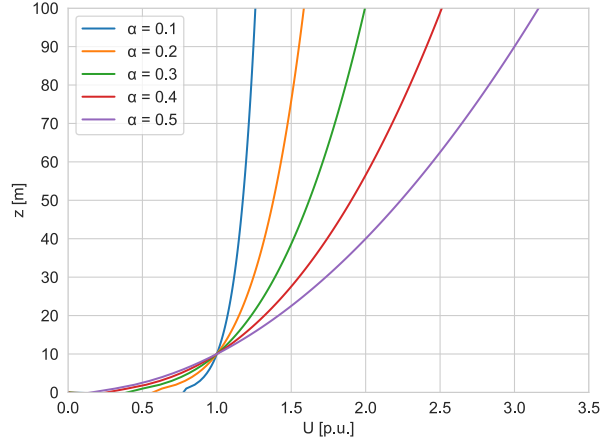
Figure 2.2: *Expected wind profile for various share exponents [7]*

2.4 Method of Bins

The method of bins is a practice used to summarize wind data and calculate turbine productivity. By separating a set of data into different bins, like wind velocity, machine production can be analyzed for each bin individually. If a set of data is separated into N_B number of bins, ideally the same size, and f_i number of occurrences, then the total number of occurrences N is given by equation 2.12. [2]

$$N = \sum_{i=1}^{N_B} f_j \tag{2.12}$$

Suppose that each bin has a midpoint m_i with width w_i, then the average wind velocity $\bar{U}$ can be derived from equation 2.3 as shown in equation 2.13. The standard deviation of the wind velocity can in the same manner be derived from equation 2.4, as shown in equation 2.14. [2]

$$\bar{U} = \frac{i}{N} \sum_{i=1}^{N_B} m_i f_i \tag{2.13}$$

$$\sigma_U = \sqrt{\frac{1}{N-1}\left(\sum_{i=1}^{N_B} m_i{}^2 f_i - N(\bar{U})^2\right)} = \sqrt{\frac{1}{N-1}\left(\sum_{i=1}^{N_B} m_i{}^2 f_i - N(\frac{i}{N}\sum_{i=1}^{N_B} m_i f_i)^2\right)} \tag{2.14}$$

3 Methods

Raw data from measurements can often be challenging to interpret. Whether it is missing data points, a general lack of order or an unfitting sampling rate, various factors can make a data set less useful. This section describes system components, raw data available from LIDAR and turbine, and how it was processed. After filtering, re-sampling and averaging data over a time interval of ten minutes, the LIDAR and SCADA data were matched. Timestamps for data not found in both data sets were dropped as wind shear is calculated by the LIDAR, and the turbine's SCADA system logs power production. Simulations were run in Ashes to compare and validate results.

3.1 Wind Turbine Characteristics

3.1.1 Wind Turbine Specifications

The wind turbine analyzed in this thesis is classified as an IEC IIA turbine. This is a classification done by IEC, describing some of the turbine and turbine site's characteristics. This wind turbine has an average wind velocity of 8.5 m/s at hub height, with a survival wind velocity of 59.9 m/s. The site has a high turbulence intensity of 16%, indicated by the letter A. This is a multi-megawatt wind turbine with hub height 94 m above ground level. The rotor has a diameter of 112 m, sweeping over 9852 m^2 when in operation. [10]

3.1.2 Pitch Control and Direction Section Management

Controlling a wind turbine is necessary to ensure a long lifespan and efficient performance. Different methods or techniques in control systems guarantee safe operation, optimized power output, and minimized structural load. [11]

Pitch control is a type of aerodynamic torque control widely adapted in the wind industry. Rotating blades about their long axis make it possible to change rotor efficiency and torque. Varying the angle of attack will change a blade's geometry influenced by wind, affecting lift and drag forces. Reducing the angle of attack will rotate the blades to a feather position while increasing the angle of attack will rotate the blades to a stall with both positions reducing loads. Varying the pitch angle between feather and stall can optimize the power coefficient by maintaining the rated rotor velocity, or reduce the power coefficient and hence the power output if necessary. [11]

Direction section management, on the other hand, is a control strategy used on the specified turbine to limit fatigue damage. This strategy is applied whenever the turbine is placed downstream from another turbine or because of complex terrain, creating turbulent airflow. Wind interacting with turbine blades during operation will create swirling vortices behind the rotor plane. These swirling vortices produce a wake downstream, which increases turbulence. This can have significant effects on other turbines placed downstream, like reduced power output due to lower mean wind velocities, increased turbulence loading leading to higher wear on turbine parts, and can affect pitch control in undesired ways. [11]

Direction section management limits power production for high wind velocities from a given direction. Another wind turbine is placed about 260 meters west for the given turbine. Power production is therefore limited by the turbine's control system for winds coming from the west between 225° and 285°, with a wind velocity $\geq 15.5 m/s$.

3.2   Wind Turbine Instrumentation and Data Analysis

3.2.1   System Components

Ultrasonic Anemometer

Two ultrasonic anemometers are mounted on top of the cooling system of the wind turbine's nacelle, feeding the turbine's control system with data. Unlike mechanical sensors, these devices use ultrasonic sound waves to measure wind velocity and direction. Wind velocity is calculated based on the time of flight of ultrasonic pulses between pairs of transducers. By combining signals from sensors, it is possible to measure one-, two-, or three-dimensional flow, typically with a resolution of 20 Hz or more. The two ultrasonic anemometers can be seen in figure 3.1. [2]

Figure 3.1: *Two ultrasonic anemometers and LIDAR mounted on top of the nacelle. Picture by Lina Nordaune*

LIDAR

One LIDAR (Light Detection and Ranging) is also mounted on top of the wind turbine's nacelle, as shown in figure 3.1. In contrast to conventional anemometers, LIDARs are classified as remote sensing devices, as they do not need an active sensor at the point of measurement. Beams of light are emitted from the LIDAR and are scattered back after interacting with air at a given distance. The light reflected is analyzed to calculate the velocity and direction of the particles from which it was scattered. These calculations are relying on the measurement of Doppler shift or change in the frequency of radiation scattered by aerosols carried by the wind. [2]

There are currently two commercial LIDAR systems being used in wind turbine applications. Both types can measure three-dimensional wind fields at a distance of up to 200 meters. The first system is a pulsed LIDAR with fixed focus, and the second being a continuous wave with variable focus design. Both these systems have shown the ability to perform measurements with a high degree of accuracy. [12]

WindVision™

The LIDAR installed on top of the turbine is a four beam WindVision™ from Windar Photonics. This device uses a continuous wave design to measure the Doppler shift between emitted and backscattered light along four different

lines of sights. At each beam, local wind velocity and direction are measured. These four measurements are used to calculate effective wind velocity and direction at hub height, as explained later in this section. WindVision™ should ideally be set to measure at a predefined distance of 2/3 of the turbine's rotor diameter. In this case, the LIDAR is set to measure at a distance of 100 meters in front of the turbine. The four beams are arranged in half-cone angles α of 18° (not to be confused with shear exponents), as illustrated in figure 3.2. [13, 14]
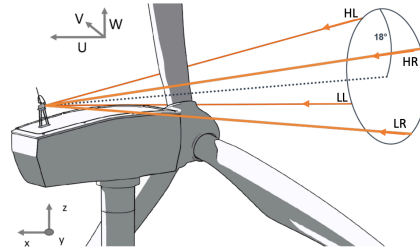
Figure 3.2: *LIDAR measuring wind velocity at four lines of sight [13]*

A half-cone angle of 18° results in a 26° opening angle between each beam, as shown in figure 3.3. Measuring at a distance of 100 meters with the given opening angle will cover an area of 46.2x46.2 square meters, between 74.4 m and 120.6 m above ground level. By creating a three-dimensional wind profile between two and two beams, this device can detect yaw misalignment and wind shear, which can improve pitching. These properties will supposedly increase AEP and reduce loads affecting the turbine. [13, 14]
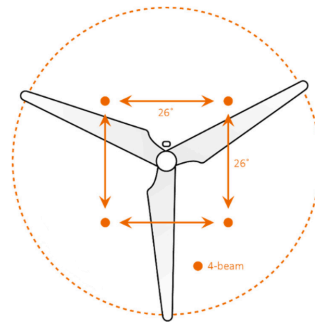
Figure 3.3: *LIDAR measurement area in front of the rotor, with a 26° opening angle [13]*

The raw LIDAR data contains measurements for each line of sight as well as three-dimensional vector profiles for wind velocity at two different heights, with U-, V- and W-components. This data makes it possible to derive wind velocity at different heights, given some realistic assumptions. [13]

Estimating average wind velocity at hub height is done with one simple assumption, that the longitudinal wind component U is prevailing the transversal and vertical wind components V and W. This means that V and W are assumed to be zero. As the LIDAR is horizontally aligned with the nacelle, the effective wind speed at hub height, U_{eff}, can be calculated from equation 3.1. Here i is ranging from 1 to 4, indicating the four line of sights HR, HL, LR, and LL. [13]

$$U_{eff} = \sum_{i=1}^{i=4} \frac{U_{los_i}}{4cos\alpha} \tag{3.1}$$

Deriving local wind velocity and direction from the two upper beams and two lower beams separately, two assumptions needs to be made. Firstly, the vertical component W is still assumed to be zero at each height. And secondly, the local wind is assumed to be homogeneous in the transversal and longitudinal direction. Meaning $U_{Right} = U_{Left}$ and $V_{Right} = V_{Left}$. Local wind velocity and direction can then be calculated from equation 3.2 and 3.3. [13]

$$U_{local} = \sqrt{u^2 + v^2} \tag{3.2}$$

$$\phi_{local} = tan^{-1}\left(\frac{v}{u}\right) \tag{3.3}$$

The components u and v are derived from equation 3.4 and 3.5. Here α' is the projected half opening in the x - y plane shown in figure 3.4, while λ is the projected half opening in the x - z plane shown in figure 3.5. Both α' and λ are set to $13°$. The tilt angle of the LIDAR θ is $0°$. [13]

$$u = \frac{U_{los_R} + U_{los_L}}{2cos(\alpha')^2} \tag{3.4}$$

$$v = \frac{U_{los_R} - U_{los_L}}{2sin(\alpha')cos(\lambda)} \tag{3.5}$$
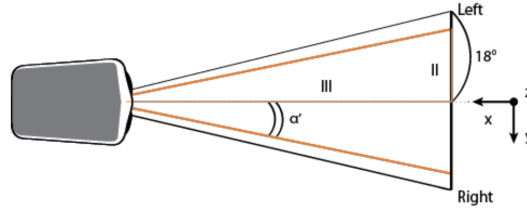
Figure 3.4: *Top view of WindVision^{TM}[13]*
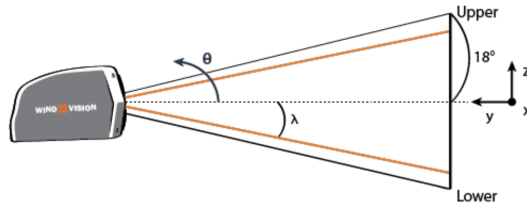
Figure 3.5: *Side view of WindVision^{TM}[13]*

3.2.2   Measured Data

Available SCADA Data

The turbine's control system, often referred to as supervisory control and acquisition, or SCADA, can initiate, shut down and coordinate operation with other wind turbines. This system relies on sensory information from the ultrasonic anemometers, among other devices, to control power production. Data collected by the SCADA system is referred to as SCADA data. The SCADA data gathered from the turbine analyzed in this thesis include;

- Active Power
- Wind Velocity

- Pitch Angle
- Wind Direction

- Nacelle Direction
- Rotor Speed

The turbine rotor influences wind velocity and direction measurements. When in motion, rotor blades create wake and shading for the anemometers located on top of the nacelle. For these effects to be eliminated, the anemometers would have to be placed more than ten times the rotor diameter downstream, or in front of the rotor plane, upstream. Locating measurement devices ten times the rotor diameter downstream would remove inaccuracy caused by the turbine rotor, but would instead introduce uncertainty caused by local variations in the wind field. Locating anemometers upstream would eliminate all these effects, but is usually expensive due to structure related costs. This is solved by running raw anemometer data through a transfer function accounting for rotor effects. The output gives a more realistic representation of the wind profile in front of the rotor plane. Wind velocity and direction is, therefore, not considered raw data. [2]

Nacelle direction is referred to $0°$ north, with wind direction referred to the nacelle direction. Data from the turbine's SCADA system is saved with a logging rate of 0.2 Hz or every five seconds. However, the nacelle direction and pitch angle are only logged when changing. The reason for the low logging rate is due to the vast amounts of data form different turbine sensors. Recording too large amounts of data is not expedient over longer periods. The SCADA data analyzed is logged between 01.10.18 and 16.01.20, with more than 25 million data points.

Available LIDAR Data

The WindVision LIDAR from Windar Photonics can measure several variables. The setup used in this thesis logged information with a sampling rate of 1 Hz, including;

- LOS Wind Velocity
- LOS Wind Direction

- LOS Status
- Number of Measurements

- Doppler Spectrum Peak
- 3D Vector Components

Wind velocity is measured for each line of sight (LOS) separately, as shown in figure 3.2. Wind direction is calculated using the two upper and two lower beams and is relative to the nacelle and LIDAR direction. Three-dimensional vector components for the lower and higher wind profile are logged by combining the two lower and two higher beams, respectively. The system also records the Doppler spectrum peak, the number of measurements done, and the reliability of these measurements indicated by a binary status. Data analyzed in this thesis was measured at varying time intervals between 26.04.2019 and 24.12.2019.

3.2.3 Data Processing

Processing SCADA Data

SCADA data available from the test turbine was downloaded as a text file holding seven different columns of data. The first column contained a timestamp format of "dd-mm-yyyy hh:mm:ss.fff", working as an index for the measurements done. The remaining six columns consisted of scalar values of variables listed in section 3.2.2. These variables were converted to a Pandas data frame in Python and sorted by timestamp before averaged over a time interval of ten minutes. The ten-minute average is chosen by convention in wind engineering and hence also used in this thesis. [2] The original data set contained numerous empty data points. Averages not containing more than 95% of expected measurements per time interval were dropped. Empty data points for blade pitch and nacelle direction was filled with last measured value as these are only logged when changing.

Data logged with extreme pitch angles were also dropped when resulting in unusually low power production. As explained in section 3.1.2 pitch control can reduce power output when desirable. A few instances of large pitch angles, high wind velocities, and low power output indicated that pitch control was used to reduce load. Eliminating these data points for an under-performing wind turbine was essential for the reliability of results. Data was, therefore, dropped if pitch angle deviated more than three times the standard deviation for mean pitch angle at every 1 m/s wind velocity, and corresponding power output was reduced. Just over 3% of the data was dropped due to the turbine under-performing.

Processing LIDAR Data

Available LIDAR data was downloaded as .dms files and converted to a separate data frame in Pandas. The data set was indexed by a timestamp similar to the SCADA data. Figure 3.6 illustrates how the four beams emitted from the LIDAR are measuring wind velocity and direction at different positions. The elevation angle γ is set to $45°$. Because of the LIDAR being placed behind the turbine's rotor, the data is influenced by the blade's shadowing. Every time one of the beams hit a rotor blade, the resulting measurement will be incorrect. This problem is increasing with the rotor speed decreasing, as the time it takes for a blade to pass a line of sight increases. The WindVision^{TM} LIDAR is always logging a binary status per measurement for each line of sight, indicating if a measurement is reliable or not. Two main conditions filtered the LIDAR data: the status of any line of sight, as well as the velocity measured, had to be non-zero.
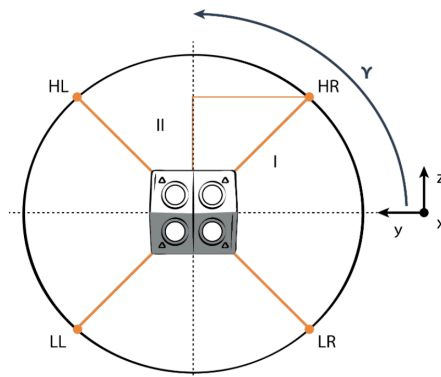
Figure 3.6: *WindVision^{TM} with four LOS and elevation angle $\gamma = 45°$ [13]*

The data frame was expanded with new columns for the effective wind velocity U_{eff} and local wind velocities U_{high} and U_{low}, following the methods given in section 3.2.1. By utilizing the power law in section 2.3.2, U_{high}, U_{low}, and their respective heights were matched to estimate shear roughness α for each measurement, defining their shear profile and extending the data frame with another column.

After calculating desired velocity and shear variables, data were averaged over a time interval of ten minutes, matching the SCADA data format and dropping any sub data sets with less than 90% of expected data points. Turbulence intensity was estimated using the mean effective wind velocity and corresponding standard deviation for all averaged measurements, as shown in section 2.2.1. LIDAR data was favored over anemometer data when calculating turbulence intensity because of a higher sampling rate.

Matching and Analysing Data

Since wind shear and turbulence intensity were calculated with LIDAR measurements, and power output was logged by the SCADA system, all data was validated by timestamps. Data without matching timestamps from LIDAR and SCADA data were therefore dropped. Due to lack of LIDAR measurements, a large part of available data was dropped, leaving a data frame of 59 days of useful data, split into approximately 8500 ten minute averages.

Data was binned between four different shear exponents, using the method of bins. This was done to analyze how different share profiles affect wind turbine characteristics, including wind velocity distribution, power output, and power coefficient. Already binned data were binned by wind velocity intervals of 1 m/s to determine power curves for all four ranges of shear profiles. The annual energy production was estimated for varying shear coefficients by combining annual wind distribution with calculated power curves. Results are presented in section 4.3.

The same approach used for analyzing how wind shear affects power production was applied to the turbulence intensity data, binning data into four ranges of turbulence intensity. Wind velocity, power curves, and power coefficients were calculated and plotted before annual energy production again was estimated. How turbulence affect power production is presented in section 4.4.

3.3 Simulations

3.3.1 About Ashes

Ashes is a simulation program for wind turbines, developed by Simis, a spin-off company from the Norwegian University of Science and Technology established in 2013. This program can simulate how a wide variety of different factors affect wind turbine performance. Wind shear, turbulence, yawed inflow, and steady winds are examples of models supported by Ashes. This thesis explores the wind shear and turbulence models. [15]

Ashes utilize a finite element method in conjunction with a co-rotational formulation of beam elements to determine the dynamic response of structures. The co-rotational formulation leads to accurate results in arbitrarily large displacements and rotations of space. Ashes will automatically choose the most fitting solver based on the analysis type, model, and characteristics of the load cases. Forces like centrifugal forces are taken into consideration and applied to the blade naturally, while other forces can be neglected with a change in settings. The Newton-Rahpsons method can be used for iterative purposes while investigating if nonlinear effects are of interest. If nonlinear effects are insignificant, Ashes will use linear solutions of equations of motions. Ashes also use blade element momentum theory,

or BEM, to determine the aerodynamic loads, which is connected to structural responses. Blades can be regarded as stiff objects or have the attributes of real blades. [15]

This simulation tool considers various types of possible losses, like tip losses when doing calculations. Phenomena such as wave loads are computed with the Morison equation and are also connected with structural responses. Buoyancy loads can both be linear and nonlinear. The turbine is by default controlled with a PI-controller, which main functions are to control generator torque and blade pitching. The program's interface is built on the Qt framework, and OpenGL is used to visualize 3-D models of wind turbines. An intuitive interface combined with advanced controls made Ashes the simulation tool of choice. [15]

3.3.2   Parameters and Specifications

Simulations run in Ashes with varying wind shear and turbulence was performed on the default wind turbine, as shown in figure 3.7. This is a three-bladed 5 MW NREL wind turbine. The default dimensions were kept as the trend for various wind shears and turbulence intensities are expected to be the same for large multimegawatt turbines. By default, the supporting tower height is set to 87.6 m, with a rotor diameter of 125.89 m, and a sweeping area of 12447 m^2. The cone angle was set to 2.5°, with the target power coefficient set to 49%, and rated RPM set to 12. The airflow in these simulations holds standard values at sea level, with the temperature set to 15°, air density set to 1.225 kg/m^3, and atmospheric pressure equal to 1 atm. Dynamic and kinematic viscosity are $1.81 \cdot 10^{-5} kg/ms$ and $1.478 \cdot 10^{-5} m^2/s$ respectively.
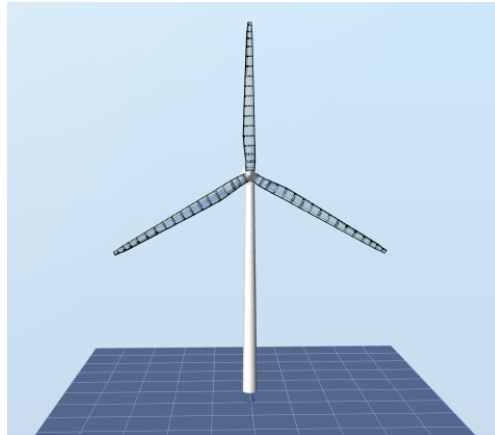
Figure 3.7: *The 5 MW NREL wind turbine used for simulations in ASHES*

Simulations were run with generator settings set to variable-speed or PID control. Variable speed control makes the wind turbine operate over the entire RPM range while also utilizing pitch regulation. The PID control adjusts torque to maintain the rated RPM of the generator. Most of the simulations were done with a linear flow, meaning that wind velocity gradually increased over time, as opposed to uniform flow. Linear flow was chosen since Ashes does not have an own method to plot power output against wind velocity, creating a power curve. Plotting power output versus time with a wind velocity increasing linearly, however, allowed for the calculations of a power curve. [15]

Ashes has configurations that allow for different types of analysis. The three options are dynamic, static, or loads only. Dynamic analysis is the only option that accounts for Newton's second law and elasticity of structures. Static

analysis neglects these characteristics, while the loads only option uses a fixed rotational velocity to run calculations. Ashes describe the dynamic option as the most realistic choice of analysis with a continually changing RPM and structural motion. Dynamic analysis was therefore used for all simulations. [15]

3.3.3   Wind Shear

An essential implementation in Ashes when interpreting power curves for various wind shears are what is known as regions. These regions are divided into five, between 1 and 3, with steps of 0.5. Region 1 is a control region before cut-in wind velocity. In this region, no power is produced, the generator torque is zero, and energy is used to accelerate the turbine rotor. Region 2 is also a control region with the goal is to optimize energy capture. The generator torque is proportional to the square of the filtered generator speed to maintain optimal TSR. In region 3 the generator power is constant, which makes the torque of the generator inversely proportional to the filtered generator velocity. Regions 1.5 and 2.5 are linear transition regions between 1-2 and 2-3, respectively. Region 1.5 functions as a start-up region, which limits the generator velocity, which effectively also limits the operational speed of the wind turbine. In region 2.5, the torque slope corresponds to that of an induction machine. This limits the tip speed at the rated power of the wind turbine. [15]

The region configurations greatly influence the simulations. Default settings make the generator move from region 1 to region 1.5 when 57.08% of rated generator RPM is achieved. This is the reason why none of the simulations produce any power before the turbine has ramped up rotational velocity considerably, as seen around 6 m/s in figure 4.8, in results. When the generator reaches 74.21% of rated RPM, region 2 is reached, as seen around 10 m/s. At 99% of rated RPM, the generator transits from region 2.5 to region 3. In region 3 the power output stabilizes at rated power, which is 5 MW in this case. [15]

Simulations were done for five different shear exponents, ranging from 0.0 to 0.4. The wind velocity at hub height was increased linearly over ten minutes to achieve smooth power curves. Results are presented in section 4.2.

3.3.4   Turbulence Intensity

Turbulence simulations in Ashes are a bit more complicated than the ones run for wind shear. Ashes provide a graphical user interface for an external turbulence generator. The turbulence generator used in these simulations is TurbSim, an open-source program developed by NREL. This simulation tool utilizes a statistical model to simulate a time series of three-dimensional wind profiles numerically. This is done at points in a two-dimensional vertical grid, which is fixed in space. TurbSim is based on SNLWIND created by Paul Veers. SNLWIND applies the Sandia method to generate a full-field turbulent wind stream component U, perpendicular to the wind turbine's rotor plane. TurbSim has been adjusted to include V and W components by using a modified version of the Sandia method to generate time series based on spectral representations. Ashes allow for the use of two different IEC spectral models; the Kaimal- and the Von Karman model. The IEC Kaimal model, as presented in section 2.2.2, was chosen for the following simulations. Ashes support three different turbulence intensities for the Kaimal model. These are categorized by letters A, B, and C, as explained in section 2.2.1. [8, 15, 16]

After choosing a model, Ashes finds the correct standard deviation for corresponding components for the given turbulence and spectral model. TurbSim creates a .sum file with input parameters and standard deviations. It then generates the random numbers needed to calculate spectral and transfer function matrices, defined in the frequency

domain. An inverse FFT is performed on the spectral components to produce time series. A random seed was not set for these simulations, although an option in Ashes. [8, 15]

Ashes do not allow for turbulence simulations with increasing wind velocity. To eventually end up with simulated power curves, simulations were done between 3 m/s and 12 m/s with a stepwise increase of 1 m/s for all three TI categories. The two-dimensional grid over the rotor plane was kept at the default settings of 1.1 times the rotor area, with 32 measurement points vertically and horizontally. Each simulation was set with an initial RPM of 10, to reduce the time of turbine power ramp-up. Other parameters were kept as previously described. Simulations were run over 10 minutes (excluding ramp-up) and exported to Excel before average power output was calculated. These calculations resulted in power curves binned by turbulence intensity, as presented in section 4.2. Figure 3.8 shows a typical turbulence simulation over 450 seconds for a wind velocity of 6 m/s.
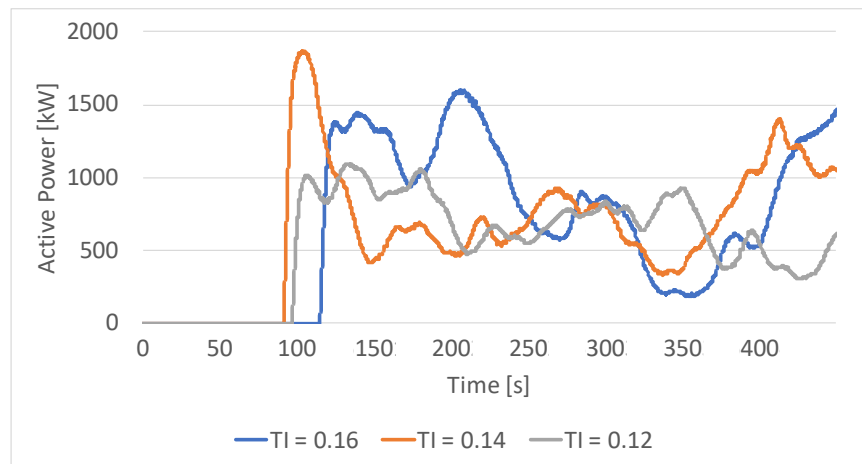
Figure 3.8: *Turbulence simulation in Ashes for 6 m/s over 450 seconds*

4 Results

This section presents the results gained from the data collected and processed. With data from the SCADA system and LIDAR filtered and re-sampled to ten-minute averages, a large amount of data was dropped due to a lack of matching timestamps for the filtered data. The measurements described in this section contain a total of 59 days of valid data centered around May and June of 2019, with a smaller subset from November and December of 2019.

4.1 The Wind Resource

Averaged wind velocity from SCADA data was plotted and compared with wind velocity calculated from LIDAR data. Figure 4.1 shows the comparison between ultrasonic anemometer and LIDAR measurements over 24 hours from June 22, 2019. The former tended to be higher than the latter. Local variations in the wind field will affect the real-time measurements as there are 100 m in between the two points of measurement, but this should be canceled out over ten minutes. Figure 4.2 shows a regression plot done on the scatter between wind velocity measured by the ultrasonic anemometer and the one calculated from LIDAR data. The blue line represents a regression done on the spread between LIDAR and ultrasonic anemometer data. The blue dashed line represents ideal LIDAR versus anemometer data. If LIDAR and ultrasonic anemometer data were to coincide, the scatter plot in orange would follow this dashed line.
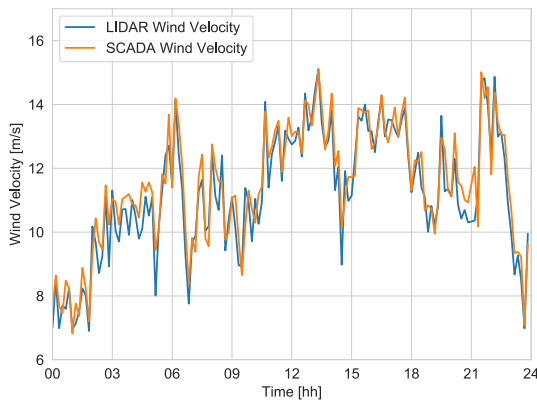
Figure 4.1: *SCADA and LIDAR wind velocity over 24 hours from June 22, 2019*
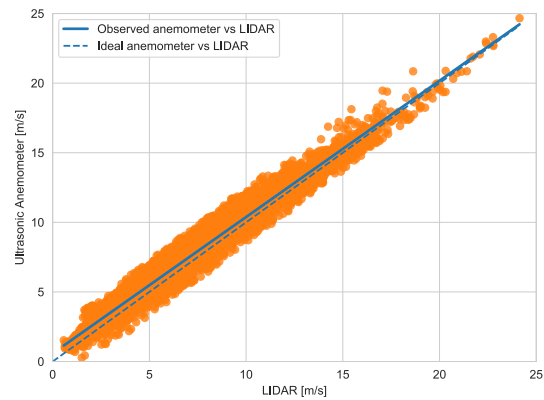
Figure 4.2: *Regression plot between ultrasonic anemometer measurements and LIDAR calculations*

The linearization in figure 4.2 is leaning towards the ultrasonic anemometer. Meaning measurements from this device often were higher than from the LIDAR. The ultrasonic anemometer measured an average of 6.48 m/s with an std of 3.66 m/s, while the LIDAR measurements averaged 6.02 m/s with an std of 3.68 m/s. This difference seems to cancel out with higher wind speeds, but this trend might be subject to fewer measurements done at wind velocities above 15 m/s.

As shown in section 3.2.3, two local longitudinal wind velocities were calculated for the upper and lower beams of the LIDAR. Figure 4.3 shows wind velocities calculated at 74.4 m and 120.6 m over 24 hours, also from June 22, 2019. The velocity estimated at 120.6 m tended to be higher than the one calculated at 74.4 m. However, almost one-fourth of the data showed the opposite, creating negative wind shear.
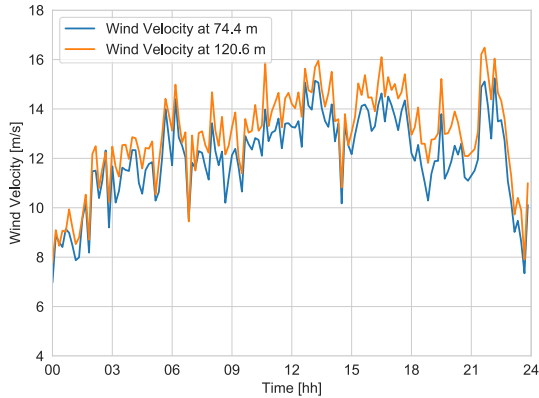
Figure 4.3: *Mean wind velocity at 74.4m and 120.6m over 24 hours from June 22, 2019*
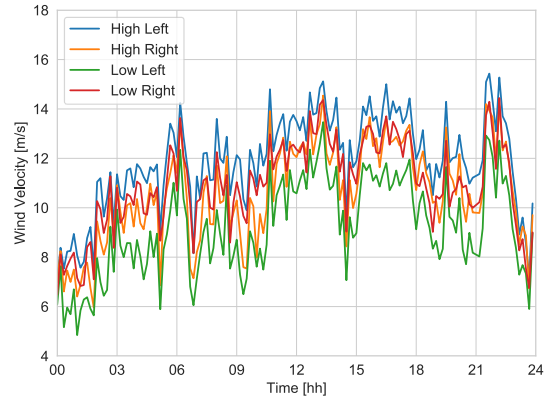
Figure 4.4: *Mean wind velocity for all four LOS over 24 hours from June 22, 2019*

Figure 4.4 shows LIDAR measurements done by the four different lines of sights used to calculate local high and low wind velocity for the same date. Using local high and low wind velocities from the WindVision™ different wind profile shear exponents were calculated, ranging from -0.5 to 0.8.

Figure 4.5 illustrates data binned by wind direction. The turbine is mainly exposed to wind from southeast, southwest, and northwest. When matching SCADA and LIDAR data, the majority of data from the southeast direction is lost due to a lack of LIDAR measurements. Why the LIDAR is less reliable when measuring in this direction is unknown. After matching timestamps, the data binned by wind direction was distributed, as shown in figure 4.6.
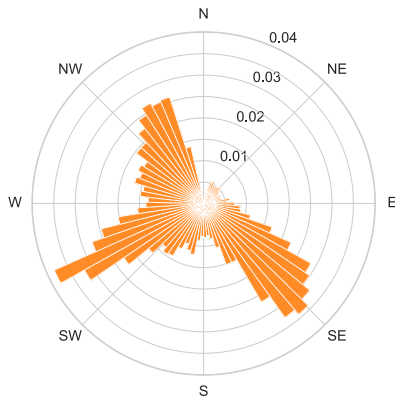
Figure 4.5: *Wind rose for unfiltered data*
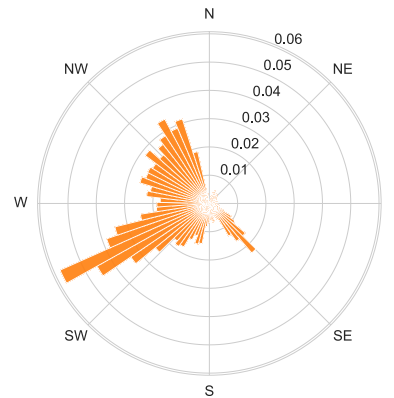
Figure 4.6: *Wind rose for filtered data*

Figure 4.7 shows percentual power production from given wind direction is plotted in blue versus the wind rose in orange from the original SCADA data. The two red lines indicate the area of section management between $225°$ and $285°$, as explained in section 3.1.2.

However, as seen in figure 4.2, wind velocities above 15.5 m/s are rarely recorded, so direction section management can only influence a fraction of the total data. Filtering the data for conditions set by DSM eliminated 1-2% of measurements, leaving almost no change to the overall calculated power curve shown later in this section.
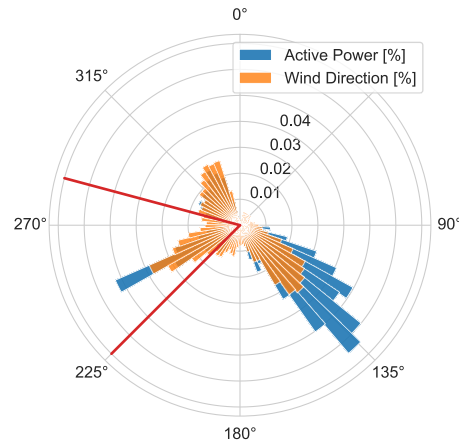
Figure 4.7: *Wind rose in orange, power distribution in blue, and DSM in red at 225° and 285°*

4.2   Results from Simulations

Simulations were run for varying shear exponents between 0 and 0.4. Since Ashes cannot generate power curves directly, all simulations were run as power output versus time, with increasing wind velocity. The wind velocity was increased linearly, making it possible to derive a power curve from the results. Simulations were exported as .txt files and converted to .xlsl files before they were processed into power curve plots in Excel. The results are presented i figure 4.8.
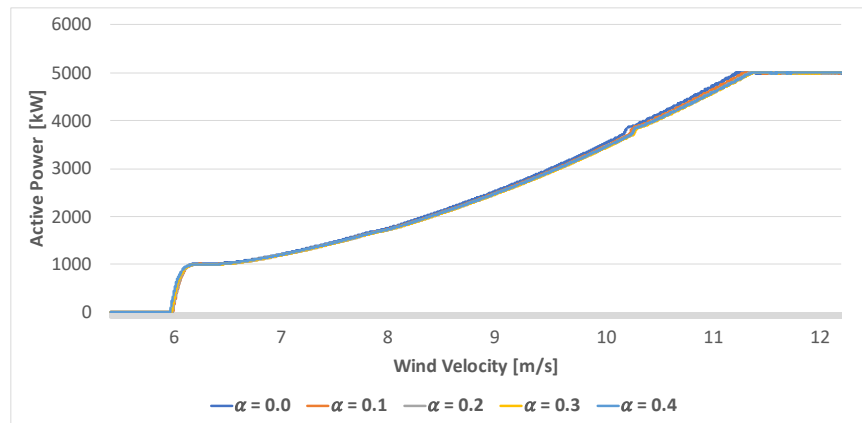
Figure 4.8: *Simulated power curves for various shear profiles*

Wind shear has a minor effect on power output. High wind shear curves are leading low or no wind shear curves for low wind velocities. This trend is reversed just before 8 m/s, where high wind shear causes the power curve to lag the reference curve with no wind shear.

As explained in section 3.3.4, turbulence simulations were somewhat more complicated. Ten-minute averages were simulated for each turbulence intensity, with wind velocity bins of 1 m/s. This resulted in mean power output for each turbulence intensity and wind velocity. This data was plotted as power curves, shown in figure 4.9.
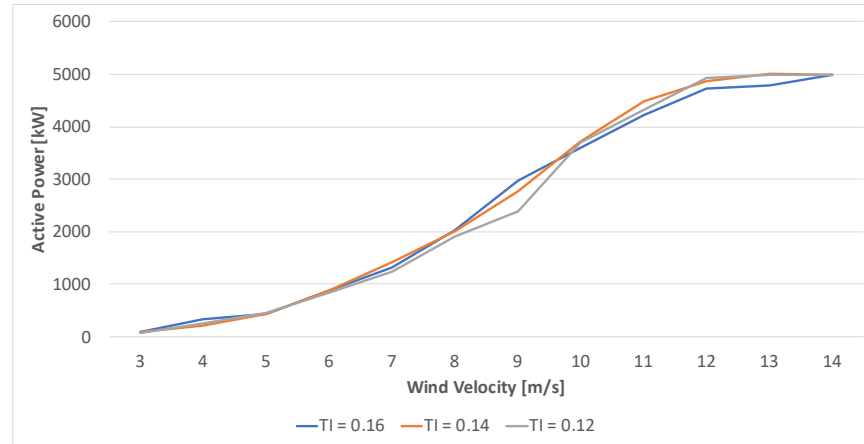
Figure 4.9: *Simulated power curves for various shear profiles*

The deviation between power curves binned by turbulence intensities 0.16, 0.14, 0.12 varies significantly with increasing wind velocity. Higher turbulence intensities have greater power output for low wind velocities. However, close to the rated wind velocity the low turbulence intensities increase power output considerably.

4.3   Effect of Wind Shear on Power Production

Using the power law to calculate a wind shear exponent for the different ten-minute averages resulted in α-values being binned in four different ranges with close to the same amount of measurements. The four ranges, as well as mean and standard deviation, are given in table 4.1.

Table 4.1: *Occurrences, mean and standard deviation for four ranges of wind shear*

Wind Shear	$\alpha < 0$	$0 \leq \alpha < 0.1$	$0.1 \leq \alpha < 0.25$	$\alpha \geq 0.25$
Occurrences	2193	1850	2069	2135
Mean	-0.157	0.050	0.168	0.468
Std	0.277	0.029	0.042	0.227

Distributions of wind velocity for different shear exponents are given in figure 4.10. By comparing effective wind speed and power output for all timestamps for any given wind shear, it is possible to compare power curves for the four ranges. Figure 4.11 illustrates a scatter plot for every instance in the existing wind data, binned by their shear exponent. Some of the measurements here are dropped for higher wind speeds with extreme blade pitch, as these measurements deliberately reduce power output for different reasons.

Using the method of bins on the already binned data was done to separate the data into more specific classes. Dividing ten-minute averages by wind velocity made it possible to calculate average power output for different wind velocities, creating a power curve. In figure 4.12, estimated power curves for the different ranges of shear exponents are drawn and compared.
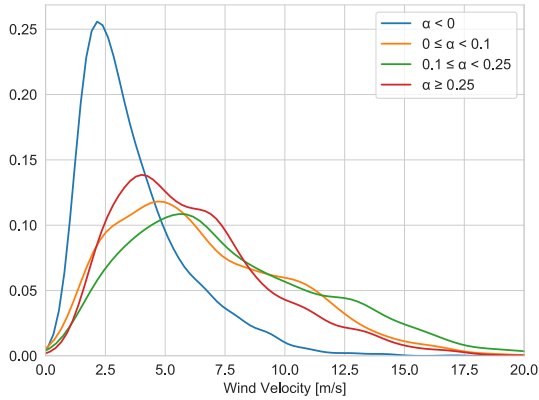
Figure 4.10: *Wind distribution for four ranges of wind shear*
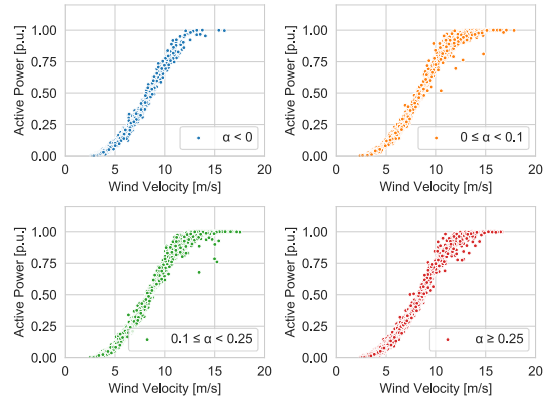
Figure 4.11: *Four scattered power curves for varying wind shear*

As explained in section 2.1, the power coefficient is a valuable property when analyzing a turbine's efficiency. Figure 4.13, illustrates how C_p, calculated with 2.1, for different shear exponents varies with wind velocity. There are no extraordinary dissimilarities between the power coefficient for different shear profiles.
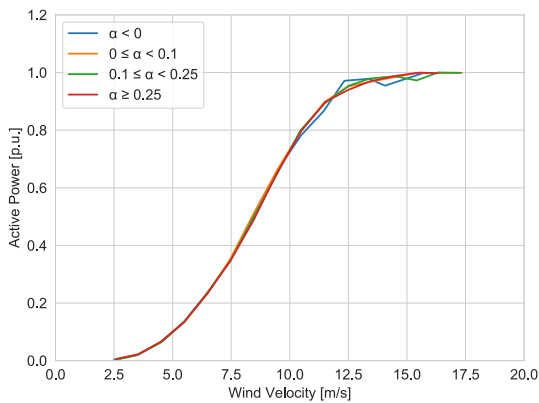
Figure 4.12: *Mean power curves for four ranges of wind shear*
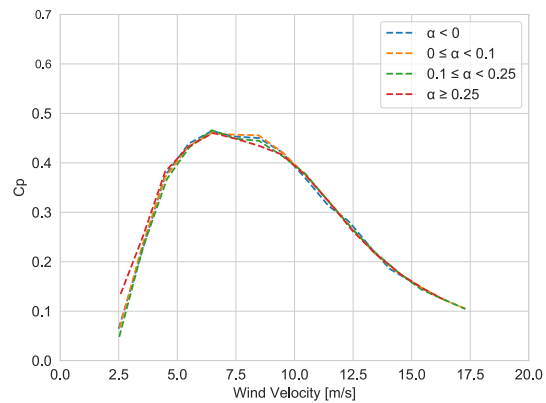
Figure 4.13: *Power coefficients for four ranges of wind shear*

Table 4.2 shows an overview of how the power curve for different shear exponents vary from the reference curve $0 \leq \alpha < 0.1$. Deviation in power output for different wind bins seems to mostly be within $\pm 3\%$, leveling off after exceeding rated wind velocity. Given that the percentual difference between shear exponents varies between positive and negative values, it is not easy to spot a clear trend. However, the overall curves are seemingly leading or higher for the reference shear exponent range.

By combining the wind distribution for an entire year, with the four power curves plotted for varying shear exponents, an AEP was calculated. Assuming that the wind distribution for the filtered data set is representative for the entire year, AEP dropped with 0.5% to 0.8% for various wind shears when compared to the reference shear exponent between 0.0 and 0.1. AEP is summarized in table 4.3.

Table 4.2: *Percentual variation in power output versus wind velocity. Reference shear exponent set to $0 \leq \alpha < 0.1$*

U [m/s]	$\alpha < 0$ [%]	$0.1 \leq \alpha < 0.25$ [%]	$\alpha \geq 0.25$ [%]
3	-6.6	-1.3	7.4
4	0.3	3.6	2.4
5	1.6	0.6	-1.0
6	0.8	1.2	1.9
7	-2.1	-2.7	-1.0
8	-0.7	-1.9	-4.5
9	-0.9	-2.3	-2.2
10	-2.2	0.1	0.0
11	-3.4	-0.6	0.2
12	2.1	0.3	-1.3
13	1.1	1.2	0.2
14	-2.9	0.4	0.6

Table 4.3: *Percentual change in AEP for varying shear exponent when compared to the reference set to $0 \leq \alpha < 0.1$*

Wind Shear	$\alpha < 0$ [%]	$0.1 \leq \alpha < 0.25$ [%]	$\alpha \geq 0.25$ [%]
AEP	-0.8	-0.5	-0.8

4.4   Effect of Turbulence on Power Production

Turbulence intensity was calculated for all measurements with equation 2.5. These calculations resulted in four different subsets of data, binned by TI. The turbulence intensity was mainly focused around 0.1, which made it difficult to bin data with an equal number of data points as done with the shear profiles. Turbulence intensity bins were therefore chosen with a fixed interval of 0.06, as shown in table 4.4, mean and standard deviation for all ranges are listed. Each range consists of a sufficient number of data points for every wind velocity.

Table 4.4: *Occurrences, mean and standard deviation for four different ranges of turbulence intensity*

Turbulence Intensity	$0 \leq TI < 0.06$	$0.06 \leq TI < 0.12$	$0.12 \leq TI < 0.18$	$TI \geq 0.18$
Occurrences	1411	3219	2214	1312
Mean	0.039	0.090	0.146	0.228
Std	0.015	0.017	0.017	0.043

Figure 4.14 illustrates wind distribution for varying turbulence intensity. This distribution is centered around low wind velocities, which reflects the overall wind distribution for the given data set. The blue and red plots suggest that both very low and high turbulence intensities are more common for low wind velocities. Power output against wind velocity is given in the scatter plot in figure 4.15. These four power curves are also binned by turbulence intensity.

Following the same procedure as done in the previous section, data binned by turbulence intensity was sorted and binned according to wind velocity and averaged for every 1 m/s. The corresponding power curves are given in figure

4.16. Between 10 m/s and 13 m/s turbulence seem to have a significant effect on power production, as power curves for higher turbulence intensities lag behind lower turbulence intensities, reaching rated power later. A clear trend is that increasing TI will reduce power output at wind velocities close to the rated wind velocity.
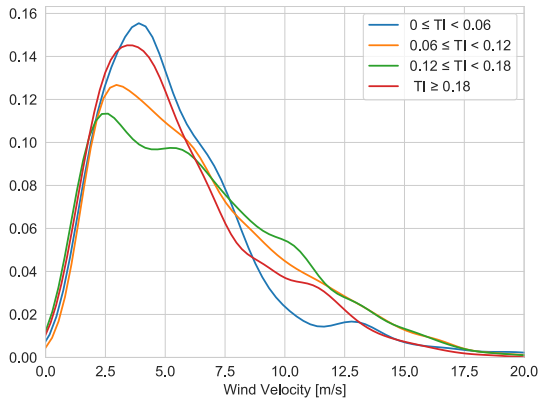
Figure 4.14: *Wind distribution for four ranges of TI*
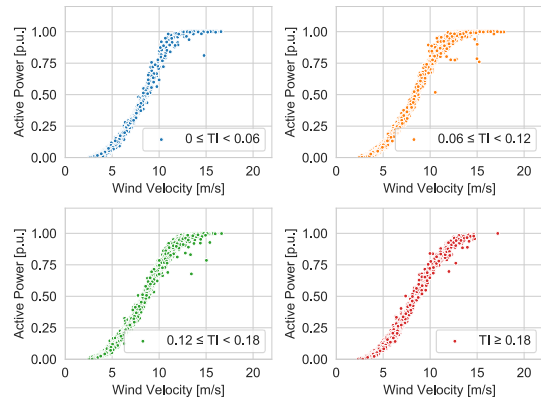
Figure 4.15: *Four scattered power curves for various TI*

The power coefficients plotted in figure 4.17 are noticeably different. C_p is higher for high turbulence wind profiles at low wind velocities. All plots are converging before the trend is reversed after 8.5 m/s. This is also where the power curves from figure 4.16 are significantly different.
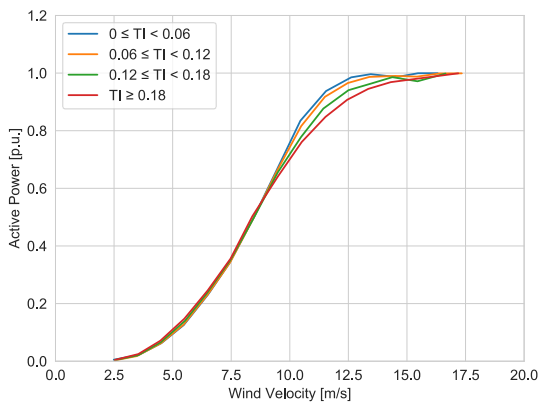
Figure 4.16: *Mean power curves for four ranges of TI*
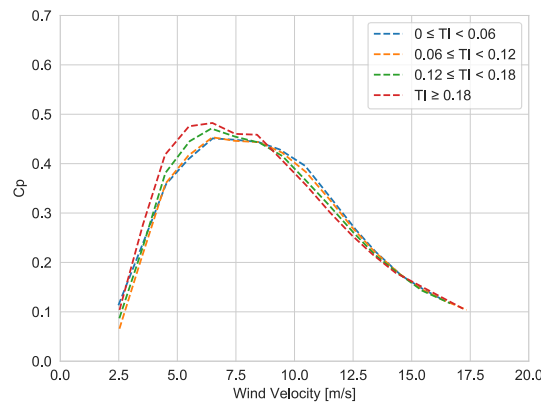
Figure 4.17: *Power coefficients for four ranges of TI*

An overview of the percentual difference in power curves are given in table 4.5, with the reference set to turbulence intensity below 0.06. Calculations done for velocities around cut-in speed are influenced by measurements done when the turbine is not in operation and may vary more than expected. The table also displays the major difference in power output between 10 m/s and 13 m/s. The deviation from the reference curve peaks around 11 m/s, with a maximum difference of 9.6% for the highest turbulence intensities.

AEP was calculated for varying turbulence intensities by combining the overall wind distribution with the respective power curves. Estimated energy dropped with 0.6% to 1.4% for increasing TI compared to the reference $0 \leq TI < 0.06$. Percentual change in AEP is summarized for various turbulence intensities in table 4.6.

Table 4.5: *Percentual variation in power output versus wind velocity. Reference turbulence intensity set to $0 \leq TI < 0.06$*

U [m/s]	$0.06 \leq TI < 0.12$ [%]	$0.12 \leq TI < 0.18$ [%]	$TI \geq 0.18$ [%]
3	-16.7	-3.6	15.6
4	-1.8	4.3	13.1
5	1.6	11.7	17.5
6	0.0	1.3	6.2
7	0.8	3.0	4.5
8	0.7	1.7	1.3
9	2.0	0.8	-1.5
10	-2.2	-6.8	-8.8
11	-2.1	-6.5	-9.6
12	-1.9	-4.5	-7.8
13	-0.9	-3.3	-5.1
14	0.4	0.0	-1.7

Table 4.6: *Percentual change in AEP for varying turbulence intensity when compared to the reference set to $0 \leq TI < 0.06$*

Turbulence Intensity	$0.06 \leq TI < 0.12$	$0.12 \leq TI < 0.18$	$TI \geq 0.18$
AEP	-0.6	-1.1	-1.4

5 Discussion

This section discusses the results presented in section 4. LIDAR and SCADA data is compared, and the reasoning behind favoring the ultrasonic anemometer over LIDAR is explained. Simulations and calculations from actual measurements are compared before LIDAR applications are discussed.

5.1 LIDAR vs. Ultrasonic Anemometer Measurements

As presented in section 3.2.1, there is a significant difference between a LIDAR and a ultrasonic anemometer. The LIDAR used in this thesis measures wind velocity and direction at four points along a circle 100 m in front of the rotor plane. Following several assumptions, effective wind velocity at hub height is calculated. The ultrasonic anemometers, on the other hand, measure wind velocity and direction directly at hub height. This data is corrected with a transfer function before it is logged. Data is recorded at different rates, with the LIDAR recording data five times as often as the ultrasonic anemometers. These differences between devices leave a room for error when comparing effective wind velocity at hub height.

When averaging wind velocity over ten minutes, instantaneous variations due to turbulence should cancel out. However, as seen in figure 4.2, LIDAR and ultrasonic anemometer averages deviate as much as 2 m/s. This inconsistency can affect results significantly. When creating power curves binned by shear exponents or turbulence intensity, choosing what device to trust was crucial for reliable results. Wind shear exponents were calculated using LIDAR data because of its ability to derive wind velocities at different heights, determining wind profiles. LIDAR data was also used to assess turbulence intensity because of its high sampling rate. However, wind velocities logged by the ultrasonic anemometers were favored over LIDAR calculations when deriving power curves for three main reasons.

Firstly, the ultrasonic anemometers are feeding the SCADA system and controlling the turbine. Anemometer data is therefore used for pitch and yaw control, to optimize power output at all times. This means that the turbine initially follows a power curve based on anemometer measurements, which is why data binned by shear exponents or turbulence intensity should do the same.

Secondly, the anemometers have shown to be much more reliable over time. This is, of course, a result of higher standards for anemometers, as they are a part of the SCADA system, controlling the turbine. The LIDAR has been inconsistent. Data is missing for months at a time and has often shown to be less reliant for high wind velocities. Figures 4.5 and 4.6 also show how the LIDAR only records a fraction of data from the southeast. The reason for less valid measurements from this direction is unknown.

Thirdly, the LIDAR uses several assumptions when performing calculations. These assumptions might have a varying effect on calculations, but figure 4.4, showing measurements for four lines of sights, indicate that they are not to be neglected. Assumptions made during calculations include $U_R = U_L$ and $V_R = V_L$. This is not the case when interpreting figure 4.4.

Results have most certainly been affected by the relatively large deviation between wind measurements. These effects were reduced by letting estimated vertical wind profiles and turbulence intensity complement the already existing SCADA data. Calculating power curves and AEP with estimated wind velocity at hub height from LIDAR data yielded unrealistic deviations in power output for varying α- and TI values. Wind velocity measured by the

SCADA system was therefore used to derive all results in section 4.

5.2   Wind Shear Measurement and Simulation Comparison

Wind shear simulations were run in Ashes as explained in section 3.3.3. It is possible to verify the results obtained from measurements, to some extent, by comparing them to the simulations. However, as simulations often are simplified, there was expected to be dissimilarities between real data and simulated ones.

Power curves for simulated shear exponents are shown in figure 4.8. This plot indicates that the changes in power output between shear exponents are minor. However, there is a trend with a decrease in power output with increasing shear profile. Power curves of wind profiles with high shear are lagging the reference power curve simulated with a uniform flow or zero wind shear. It is reasonable to assume that a wind turbine exposed to high wind shears will have a reduced AEP. The magnitude of this effect will depend on the size of wind shears, as well as wind distribution. Wind distribution concentrated around the higher end of the power curve would result in a more significant loss, as the deviations between all curves are more substantial at these wind velocities.

As explained in section 3.3.3, the different regions are affecting wind shear simulations. This is most evident around 6 m/s when the power output ramps up. In this region, high wind shear seems to have a positive effect on turbine performance, leading the reference power curve. As noted, lower wind shear generally performs better at higher wind velocities, reaching rated power before curves of high wind shear.

Wind velocity distributions were calculated and plotted, as shown in figure 4.10. There are three things to note from this plot. First of all, the mean wind speed for the entire data set is fairly low at 6.5 m/s, with relatively few occurrences of rated wind speed. Secondly, negative wind shear profiles are observed at very low wind velocities, with most cases occurring below 5 m/s. And thirdly, positive wind shear seems to have a similar distribution. Which makes it is hard to conclude if higher wind velocities cause higher wind shear or not.

The mean power curve for different shear exponents is given in figure 4.12. In this plot, the power curve for negative shear exponents is standing out. There are considerable variations for higher wind velocities. This is due to the low amount of measurements for negative shear exponents at high velocities. The three power curves for positive shear exponents follow each other seemingly closely, with a leading reference curve. This trend ceases closer to rated wind speed and is probably subject to a lower number of measurements at these velocities.

Results from wind shear measurements are relatively consistent with simulations. There are no extreme deviations between power curves binned by shear exponents. Calculated power curves differ from simulations for higher wind velocities, as simulations predict that power output will drop more noticeably for greater wind shears. Overall the power curve seems to drop in both cases, reducing AEP.

5.3   Turbulence Intensity Measurement and Simulation Comparison

Simulations were run for turbulence intensity in Ashes, as explained in section 3.3.4. Somewhat more complicated simulations were run for turbulence intensity, much due to the complexity of turbulence. These simulations resulted in the power curves shown in section 4.2.

There is a notable deviation between all three power curves at certain wind velocities. This might be a result of relatively few data points for each wind velocity. Due to the time-consuming simulation process, each turbulence

intensity binned by wind velocity only contain one ten-minute average of data. As turbulence simulations are largely based on randomness, ten-minute averages, as used by convention, could deviate more than desirable. More extensive simulations would most likely smoothen the curves.

Figure 4.9, look to be subject to a small trend, where power output is greater for higher TI values at lower wind velocities. This trend seems to reverse around 10 m/s, where the power curve for high TI drops significantly below the others. The power curve for TI = 0.16 seems to lag the two other power curves substantially when close to rated power.

The wind distribution for different turbulence intensities measured can be found in figure 4.14. This distribution is centered around low wind velocities, which reflects the overall wind distribution for the given data set. The blue and red plots suggest that both very low and high turbulence intensities are more common for low wind velocities. High turbulence intensities are expected to happen at low velocities. If the TI intervals would have been chosen differently, the wind distribution would most likely look different. However, this distribution makes it difficult to conclude if high turbulence intensities do occur more often than low intensities at low wind velocities. The scattered power curves in figure 4.15 shows that only one valid data point was recorded for TI over 0.18 at 15 m/s or higher. This indicates that turbulence intensity does reduce with higher wind velocity. Since turbulence is the ratio between standard deviation and the mean velocity, it is mathematically reasonable that TI is reduced with increasing velocity.

Power curves binned by turbulence intensity, as shown in figure 4.16, deviate significantly. High turbulence intensities, above 0.18, have a leading power curve for relatively low wind velocities. Around 8 m/s there is a new clear trend. Turbulence intensity is decreasing power output significantly for higher wind velocities.

The power coefficients plotted in figure 4.17 are also noticeably different. C_p is higher for high turbulence wind profiles at low wind velocities. All plots are converging before the trend is reversed after 8.5 m/s. After this point the the power curves from figure 4.16 are considerably different.

These results indicate a drop in AEP for more turbulent wind profiles. The magnitude of this drop will be affected by the wind distribution. A mean wind closer to rated wind speed will reduce power production more than lower mean values, as the curve deviations are the most extensive here. An exception occurs around cut-in speed. These calculations are influenced by measurements done when the turbine is not in operation and may vary more than expected. Since wind velocity is raised to the power of three when determining available power, inconsistent measurements at low velocities will influence the results to a reduced extent compared to the ones done at higher velocities.

Both turbulence simulations and calculations indicated that turbulence has a larger impact on power production than wind shear. In both cases, the power curve of the highest turbulence intensity dropped well below the ones with lower turbulence intensity for higher winds. The opposite showed to occur for lower wind velocities, where higher turbulence intensities yielded greater power outputs. Overall, simulations and measurements showed the same trends, reducing AEP for higher turbulence intensities. Consensus between simulations and calculations increased the reliability of the results.

5.4   LIDAR Applications

There is little doubt that LIDAR technology has great potential in the wind turbine industry. As mentioned in section 3.2.1, both continuous and pulsed LIDARs have shown the ability to measure wind velocity with high accuracy and

precision. However, the WindVision$^{\text{TM}}$ used in this thesis had reliability issues, as previously discussed.

This lack of reliability limits LIDAR applications for this specific turbine. According to Windar Photonics, their LIDAR can work as a part of the turbine's control system. Yet, as emphasized in this thesis, the WindVision$^{\text{TM}}$ is not suited for turbine control in these conditions. Failing to measure wind velocities as high as cut-out speed can cause severe damage. Inaccurate measurements will also increase fatigue and stress on the turbine structure, as a result of inefficient pitching.

Using a LIDAR to compliment the SCADA system is, in this case, the better option. Monitoring wind shear and turbulence intensity (although possible with anemometers too) have positive effects. As demonstrated in this thesis, wind shear and turbulence intensity affect power production. Having wind shear and turbulence intensity data for existing or potential wind turbine sites can increase precision when predicting AEP. Precise AEP estimations can help reduce risk when expanding power production and can enhance cost analysis for a given wind farm. LIDAR can, therefore, be beneficial when monitoring and predicting power production. As opposed to tall wind tower structures. This is a cost-effective and relatively easy solution to observe wind profiles.

6 Conclusion

Wind shear has been shown to affect power production from wind turbines. Simulations run in Ashes indicated that this effect was minor. High wind shear performed slightly better power outputs than uniform wind profiles for low wind velocities. This trend was reversed around 8 m/s, at this point high wind shears made the power curve drop significantly. Simulations showed that AEP would be reduced for wind profiles with high shear. Measurements and calculations done presented a similar trend to the one found from simulations. Various wind shears did not produce any extreme results compared to the reference shear $0 \leq \alpha < 0.1$. However, higher wind shears produced slightly better for low winds and worse for winds above 7 m/s. Overall, power curves for high wind shear lagged the reference shear, reducing AEP. Assuming that the wind distribution used for all calculations are representative for one year, AEP was reduced with 0.8%, 0.5%, and 0.8% for $\alpha < 0$, $0.1 \leq \alpha < 0.25$, and $\alpha \geq 0.25$, respectively.

Turbulence was shown to affect power production more than wind shear. Simulations were run for various turbulence intensities. These simulations resulted in power curves with significant deviations. High turbulence intensities performed slightly better for wind velocities under 10 m/s. After this, the power curve for TI = 0.16 dropped substantially below the reference curve TI = 0.12. Measurements found power curves binned by turbulence to perform better for high turbulence intensity at low wind velocities. Increasing turbulence intensities caused power output, however, to drop for velocities over 9 m/s. This was a clear trend that coincided with simulations. AEP dropped with 0.6%, 1.1%, and 1.4% for $0.06 \leq TI < 0.12$, $0.12 \leq TI < 0.18$, and $TI \geq 0.18$, respectively.

References

[1] The Norwegian Water Resouces and Energy Directorate. *Vindkraft NVE*. The Norwegian Water Resouces and Energy Directorate. Viewed 19.05.20. <https://www.nve.no/energiforsyning/kraftproduksjon/vindkraft/?ref=mainmenu>

[2] J. F. Manwell, J. G. McGowan and A. L. Rogers. (2009) *Wind Energy Explained*. John Wiley & Sons.

[3] Ziyad Salameh. (2014) *Renewable Energy System Design*. Elsevier Inc.

[4] Håvard Karoliussen. (2016) *Vindkraft*. Fakultetet for teknologi, NTNU.

[5] M. Lange, U. Focken. (2005) *Physical Approach to Short-Term Wind Power Prediction*. Met Office.

[6] Danish Wind Industry Association. *Roughness and Wind Shear*. Danish Wind Industry Association. Viewed 08.02.19. <http://dr\T1\omst\T1\orre.dk/wp-content/wind/miller/windpower%20web/en/tour/wres/shear.htm>

[7] A. Honrubia, A. Vigueras-Rodriguez, E. Gomez Lazaro and D. Rodriguez-Sanchez. (2010) *The Influence of Wind Shear in Wind Turbine Power Estimation*. Renewable Energy Research Institute.

[8] B.J. Jonkman. (2009) *TurbSim User's Guide: Version 1.50*. National Renewable Energy Laboratory

[9] Aeolus. *SimWindFarm Wind Field Modelling*. Aeolus. Viewed 03.05.19 <http://www.ict-aeolus.eu/SimWindFarm/model-windfield.html>

[10] Matthew Huaiquan Zhang. (2015) *Wind Resource Assessment and Micro-siting, Science and Engineering, First Edition*. John Wiley & Sons Singapore Pte Ltd.

[11] National Instruments. *Wind Turbine Control Methods* National Instruments. Viewed 16.03.19. <https://www.ni.com/en-no/innovations/white-papers/08/wind-turbine-control-methods.html>

[12] A. Honrubia, A. Vgueras-Rodriguez, E. Gomez-Lazaro, M. Mejias and I. Lainez. (2010) *Comparative Analysis Between LIDAR Technologies and Common Wind Speed Meters*. Renewable Energy Research Institute, University of Castilla-La Mancha.

[13] Aitoine Larvol. (2016) *WindVision Setup and Measurement Capabilities*. Windar Photonics A/S.

[14] Anders Lindbjerg Bak. (2017) *WindEye^{TM} and WindVision^{TM} Product Specifications*. Windar Photonics A/S.

[15] Simis AS. *Ashes User Manual*. Viewed 20.03.19. <https://www.simis.io/help/#cf652d8c958 34e10bed45fd146017781>

[16] Paul S. Veers. (1988) *Three-Dimensional Wind Simulation*. Sandia National Laboratories.